MATERIALS SCIENCE

Direct 2D-to-3D transformation of pen drawings

Seo Woo Song[1]*, Sumin Lee[2]*, Jun Kyu Choe[3], Na-Hyang Kim[3], Junwon Kang[4],
Amos Chungwon Lee[1], Yeongjae Choi[5], Ahyoun Choi[4], Yunjin Jeong[1], Wooseok Lee[2],
Ju-Young Kim[3], Sunghoon Kwon[1,2,4,5†], Jiyun Kim[3,6†]

Pen drawing is a method that allows simple, inexpensive, and intuitive two-dimensional (2D) fabrication. To integrate such advantages of pen drawing in fabricating 3D objects, we developed a 3D fabrication technology that can directly transform pen-drawn 2D precursors into 3D geometries. 2D-to-3D transformation of pen drawings is facilitated by surface tension–driven capillary peeling and floating of dried ink film when the drawing is dipped into an aqueous monomer solution. Selective control of the floating and anchoring parts of a 2D precursor allowed the 2D drawing to transform into the designed 3D structure. The transformed 3D geometry can then be fixed by structural reinforcement using surface-initiated polymerization. By transforming simple pen-drawn 2D structures into complex 3D structures, our approach enables freestyle rapid prototyping via pen drawing, as well as mass production of 3D objects via roll-to-roll processing.

INTRODUCTION

Transformation of two-dimensional (2D) planar structures into 3D structures has recently emerged as a strategy for incorporating the advantages of 2D-based technology into the fabrication of 3D objects (1–4). 2D fabrication is simple and suitable for mass production, but its output is limited to planar structures. In contrast, 3D fabrication can create tangible real-world objects with a variety of structures, but the design and fabrication processes are relatively slow and complicated. Therefore, 2D-to-3D transformation technologies can increase throughput and simplicity in 3D fabrication by constructing a complex 3D structure from easily fabricated 2D initial precursors (5–28). 2D-to-3D transformation techniques such as origami (5–11), buckling (12–16), shape memory composites (17–20), and 4D printing (21–28) are implemented by folding, bending, and assembling a 2D planar sheet into a designed 3D structure. However, the accessibility of these technologies may be insufficient because of the necessity of transformable smart materials, functional substrates, or additional instruments such as 3D printers that can print out multilayered structures required to implement their transformation mechanisms.

In 2D space, the pen is the most creative, convenient, and familiar tool for expressing one's idea. Pen drawing provides advantages related to its high accessibility, high portability, freestyle usability, and on-site manufacturability (29). These properties have led to adopting the pen to on-site and freestyle fabrication in the fields of microfluidics (30–33), flexible electronics (34–36), wearable devices (37, 38), and displays (39, 40). Moreover, the pen-based approach can be combined with existing 2D-printing systems (e.g., pen plotter) to achieve high levels of accuracy and mass producibility. Despite such advantages, pens have generally been seen as drawing tools for use only on 2D surfaces until the development of a pen-style

3D printer (41). The pen-style 3D printer provided a strategy for adopting the pen as a direct 3D fabrication tool, but controlling the pen in empty space was not as fast or convenient as using a pen on a 2D surface. For this reason, we aimed to incorporate the strengths of a 2D pen drawing into a more rapid and intuitive process for 3D fabrication by developing 2D-to-3D transformation technology that can transform a pen drawing on a 2D surface into a tangible object. Although various shape-morphing technologies have been developed previously, none has been implemented with a pen, which can be the preeminent rapid prototyping method incorporating benefits related to both freestyle usability and high throughput.

Here, we developed a "pen-based 4D printing" that enables fabrication of 3D architectures directly from 2D pen drawings simply by dipping the drawings into a monomer solution (Fig. 1, A and B). This method is based on a shape-morphing mechanism that relies on surface tension–driven selective peeling and floating of dried ink film and is referred to as surface tension–assisted transformation (STAT) (Fig. 1C). The ink of a dry-erase marker, which includes polyvinyl butyral (PVB) resin, forms a hydrophobic thin film after drying. When submersed in an aqueous solution, the PVB film detaches from the substrate as the solution penetrates the film-substrate interface driven by capillary force. The detached PVB film then floats on the solution surface due to surface tension (Fig. 1C and fig. S1). The basic principle of the capillary-induced peeling of hydrophobic thin film was studied by Stone's group and others (42–44), but practical applications of this phenomenon have been limited to the 2D-based technologies (45–48). To extend its use to 2D-to-3D transformation technology, we first introduced selective peeling and floating of the film to transform a 2D drawing into a 3D structure. As the occurrence of peeling depends on the adhesion force between the film and the substrate, we developed two types of inks having different adhesion forces by controlling the ink compositions. In this way, programmable design of 2D-to-3D transformation is available by selectively determining the floating and anchoring parts of a drawing. After the 2D-to-3D transformation of the pen drawing in response to the water level, the 3D structure of the PVB film is fixed and further strengthened by surface catalytically initiated radical polymerization (SCIRP) (49), a polymer coating process (Fig. 1C, bottom). It allows the transformed 3D object to retain its structure even after removal from the solution. As a result, the initial precursors transform its shape depending

[1]Bio-MAX Institute, Seoul National University, Seoul 08826, South Korea. [2]Department of Electrical and Computer Engineering, Seoul National University, Seoul 08826, South Korea. [3]Department of Materials Science and Engineering, Ulsan National Institute of Science and Technology, Ulsan 44919, South Korea. [4]Interdisciplinary Program for Bioengineering, Seoul National University, Seoul 08826, South Korea. [5]Nano Systems Institute, Seoul National University, Seoul National University, Seoul 08826, South Korea. [6]Center for Multidimensional Programmable Matter, Ulsan National Institute of Science and Technology, Ulsan 44919, South Korea.
*These authors contributed equally to this work.
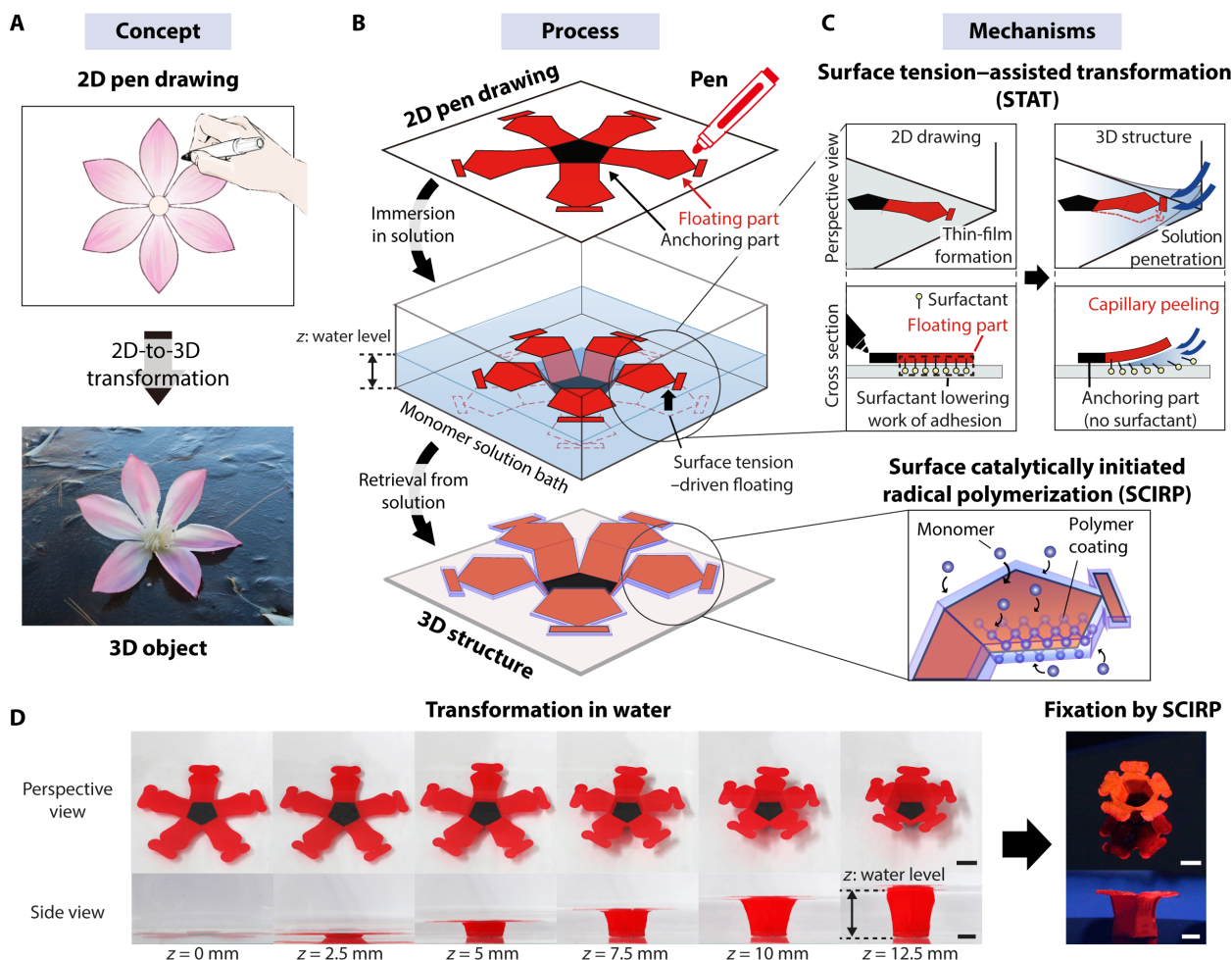†Corresponding author. Email: jiyunkim@unist.ac.kr (J. Kim); skwon@snu.ac.kr (S.K.)

Fig. 1. Pen-based 4D printing enables simple transformation of 2D pen drawings into 3D structures. (**A**) Conceptual illustration of pen-based 4D printing. Pen-based 4D printing enables simple and intuitive 3D fabrication via 2D-to-3D transformation of 2D pen drawings. (**B**) Pen-based 4D printing process. A pen is used to generate a hydrophobic thin film after the ink dries. This 2D pen drawing transforms into a 3D structure via STAT when immersed in a monomer solution. The transformed 3D shape is fixed via SCIRP during a 3-min incubation period in the monomer solution. (**C**) STAT and SCIRP mechanisms. The type of ink applied determines whether a specific part of the structure floats or is anchored. A polymer coating layer is generated around the 3D structure of the dried ink film to strengthen its architecture. (**D**) Sequential view of the 2D-to-3D transformation depending on water level. The 3D structure can be further fixed by SCIRP using a monomer solution including KPS ions (right). Scale bars: 5 mm. Photo credit: Seo Woo Song, Sumin Lee, and Junwon Kang; Seoul National University.

on the water level and can be further fixed by SCIRP by using a monomer solution including potassium persulfate (KPS) (Fig. 1D).

Shape morphing based on STAT is simple and intuitive and does not require a high technical level to predict the resulting structural transformations. Instead of bulky equipment, pen-based 4D printing only requires drawing pens and a monomer solution, thus making 3D structure formation more accessible. Furthermore, pen drawing can be integrated with conventional printing techniques to incorporate the benefits of both drawing (low cost and simplicity) and printing (mass production and reproducibility). Computer-aided design (CAD) and automatic printing systems can also be introduced for more precise fabrication or mass production (movie S1).

RESULTS
Surface tension–assisted transformation
When a 2D drawing enters the monomer solution, peeling of the PVB film depends on the thermodynamic work of adhesion (*W*)

(see Supplementary Text). Commercial dry-erase markers include surfactants that lower the *W* value of the ink (*50*), and drawings created with these markers can easily be peeled off of a substrate. We found that removing surfactants from the ink increased the *W* value, thereby preventing detachment of the film from the substrate. Using this principle, we developed a floating ink containing surfactant and an anchoring ink without surfactant that can be used to draw the floating parts and anchoring parts of a drawing, respectively (Fig. 2A, fig. S2, and movie S2). Therefore, when a drawing is submersed in the solution, only the parts drawn in floating ink with a low *W* value will peel off to form the intended 3D structure.

To determine the optimal composition of the floating ink (fig. S3), we investigated the relationship between the fracture strain of the PVB film and the weight percentages of the PVB and plasticizer contained in the ink using a nano–universal testing machine (nano-UTM) (Fig. 2B and fig. S4) (*51*, *52*). Higher concentration of PVB increased the formation of polymer chains and made the PVB film more capable of enduring deformation or fracture strain. In contrast,
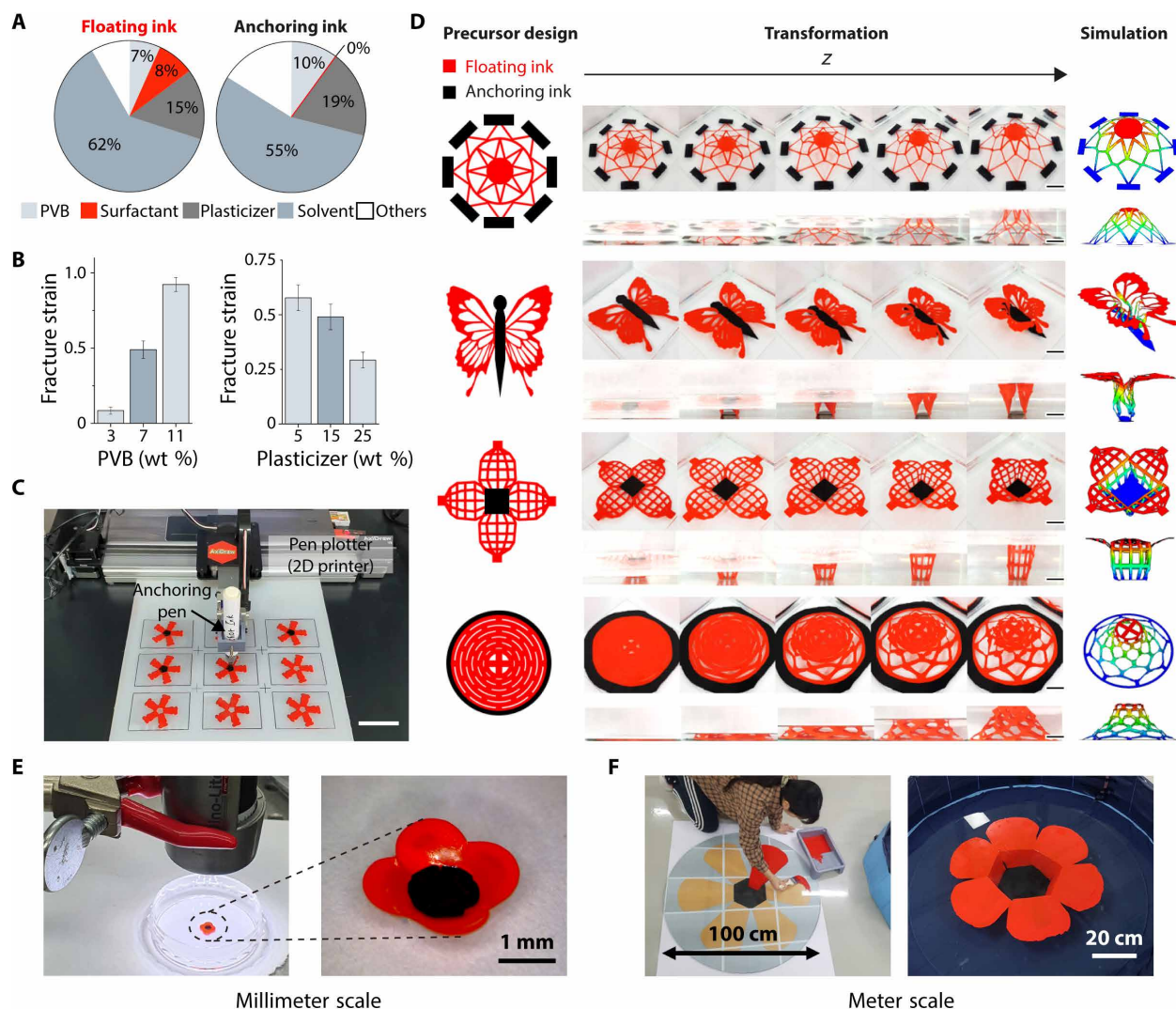
Fig. 2. 2D pen drawings can be transformed into complex 3D structures depending on water level height. (**A**) Compositions of the floating and anchoring inks. The presence or absence of surfactant determines the floating properties of the PVB film. (**B**) Fracture strain of the PVB film depending on the proportions of PVB and plasticizer in the ink (see also figs. S4 and S5). Error bars represent SD. (**C**) Pen drawing combined with an automatic printing system for precise drawing and mass production. (**D**) Sequential transformations at different water level heights as compared with simulated transformation results. (**E** and **F**) Scalability of pen-based 4D printing. (E) Millimeter scale (see also fig. S13). (F) Meter scale (see also fig. S14). Scale bars: 5 cm (C) and 2 cm (D). Photo credit: Seo Woo Song and Sumin Lee, Seoul National University; Jun Kyu Choe, Ulsan National Institute of Science and Technology.

the plasticizer is an additive that permeates the polymer chains and decreases the attraction between them. Plasticizer molecules do not combine with the polymer chain network; thus, they can be eluted out when the PVB thin film is stretched, thereby lowering the fracture strain of the film. In pen-based 4D printing, an initial precursor with high fracture strain can be transformed into more diverse structures that endure strain even in higher water levels. Meanwhile, PVB films with a higher fracture strain tend to have a lower elastic modulus (fig. S4C), making 3D architectures more vulnerable to deformation induced by external perturbation. We determined the optimal composition of the ink (Fig. 2A) by considering both the spreadability of the ink and the mechanical properties of the PVB film (figs. S4 and S5).

We used a computer-aided pen-drawing system to achieve better design precision and mass production with high reproducibility (Fig. 2C, figs. S6 and S7, and movie S3). The resolution of the drawings was determined by the size of the pen nib, making it possible to fabricate structures of various sizes (fig. S8). We presented various complex 3D structures from pen drawings by simply immersing the drawings in the water (Fig. 2D). A finite element analysis (FEA) simulation model was used to estimate the transformation morphology (figs. S9 and S10, and movie S4). In addition, we demonstrated complex transformations induced by the horizontal stress applied at the PVB film, such as kirigami (fig. S11) and serpentine structures (fig. S12). Another advantage of STAT is that it is a scalable shape-morphing method applicable to the wide range of scales. To show the scalability, we demonstrated various structures from millimeter scale (Fig. 2E and fig. S13) to meter scale (Fig. 2F and fig. S14). Unless otherwise stated, other experimental data were conducted in centimeter scale.

Structural reinforcement by SCIRP

The 2D PVB film can easily be transformed into designed, complex 3D structures using STAT. However, the structure can typically only be maintained underwater because the force maintaining the 3D structure is generated by interfacial tension between the floating part and the surface of the water. Therefore, we developed a structural reinforcement method using SCIRP to allow the 3D object to retain its structure outside the water (Fig. 3A, fig. S15, and movies S5 and S6). Our approach builds on work by Ma *et al.* (*49*) that demonstrated the formation of hydrogel coatings on a wide variety of substrate materials containing iron microparticles. For the SCIRP process, we used floating ink containing iron microparticles (5 μm) and a monomer solution containing KPS (fig. S15B) instead of the standard floating ink and water used in Fig. 2. Iron microparticles accelerate the decomposition of persulfate ions, creating free radicals near the surface of the PVB film. As a result, a polymer coating layer more than 300 μm thick can be generated around the 3D

products within 3 min, reinforcing the structure and allowing it to retain its 3D shape outside the solution (Figs. 1D and 3B and fig. S16). The stiffness of the structure increased 1000-fold after 3 min of polymer coating. By increasing the concentration of iron microparticles in the floating ink, a thicker and more robust structure was formed (Fig. 3C). Also, a gradient in the thickness of polymer coating within a single structure can be achieved by controlling the local concentration of iron microparticles (fig. S17). However, ink containing more than 50 weight % (wt %) of iron microparticles did not float spontaneously on the solution surface. Similarly, the thickness of the polymer coating layer increased according to incubation time in the monomer solution, but 3 min was enough for the structure to be maintained outside the water (Fig. 3C). As the incubation time increased, the thickness of the polymer coating increased as well, but the uniformity of the thickness decreased (fig. S18). Also, the different size of iron particles affects the speed of polymer coating and the uniformity of the coated surface (fig. S19). Considering
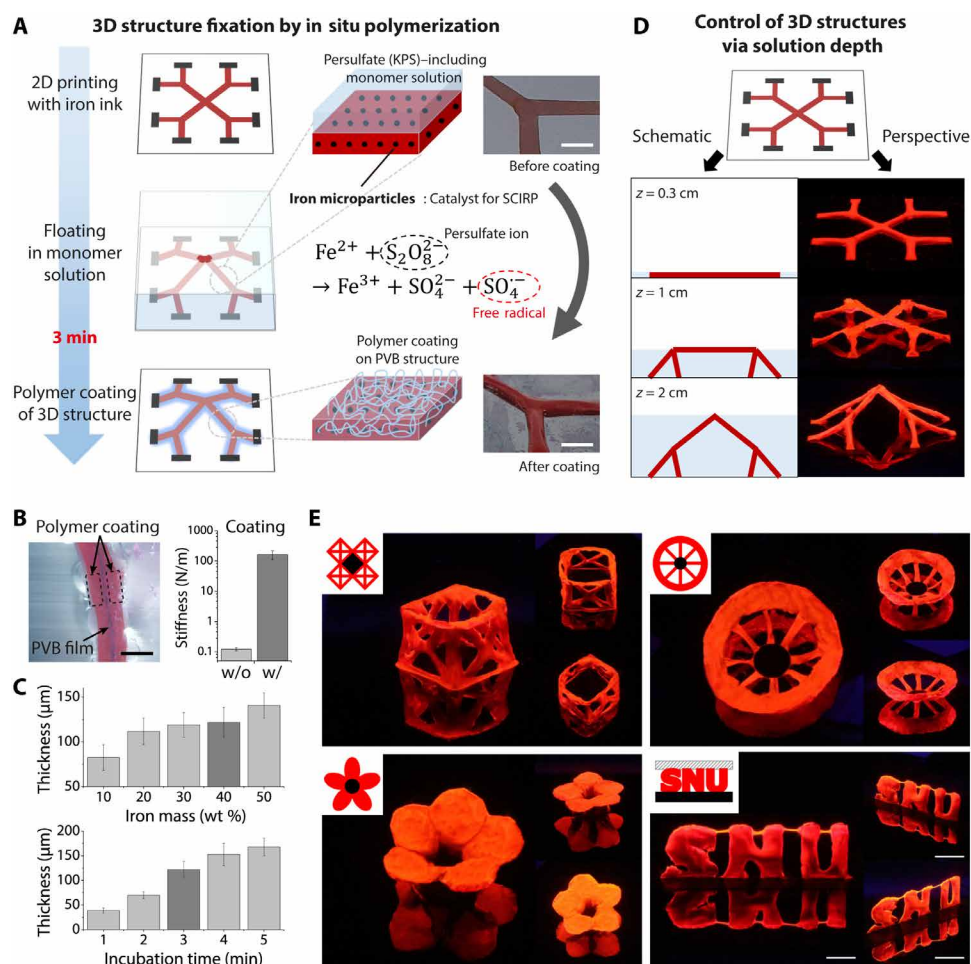

Fig. 3. Structural strengthening of transformed 3D shapes via SCIRP. (**A**) Schematic of the SCIRP mechanism. A pen-drawn precursor transforms into a 3D structure after submersion in a monomer solution. Subsequently, iron microparticles embedded in the PVB film induce local polymerization surrounding the PVB film. (**B**) Stiffness enhancement via polymer coating. Forty weight % of iron microparticles and 3-min incubation time were used. Stiffness of the structure increases 1000-fold after polymer coating as compared with the uncoated PVB film. (**C**) Dependence of the coating thickness on the iron microparticle concentration in the ink as well as on incubation time. Error bars represent SD. (**D**) Distinct 3D structures formed from the same precursor design using different solution depths. (**E**) Various 3D structures fabricated via pen-based 4D printing. Inset images show the initial precursor designs. Red and black areas were drawn by floating ink and anchoring ink, respectively. Shaded area represents sacrificial layer. Scale bars: 0.5 cm [(A), (D), and large images of (E)], 300 μm (B), and 1 cm [small images of (E)]. Photo credit: Seo Woo Song and Sumin Lee, Seoul National University.
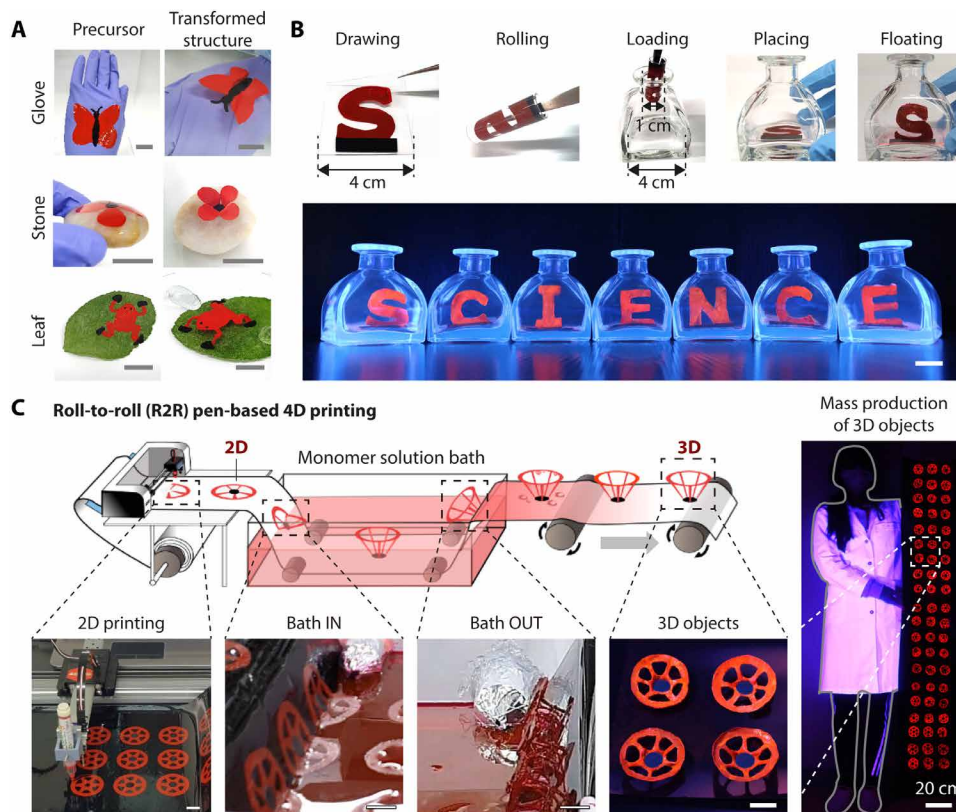
Fig. 4. Pen-based 4D printing enables "3D printing anywhere" and R2R 3D fabrication. (**A**) Pen-based 4D printing on various substrates. A pen-based approach allows the fabrication of 3D structures even on curved surfaces. (**B**) Demonstration of an "impossible bottle" construction. Drawing on the flexible PDMS film enables on-site reconfiguration of a 3D architecture inside a narrow space that would be inaccessible to conventional 3D printers. (**C**) R2R pen-based 4D printing for rapid prototyping and mass production. Quantitative analysis of the products made by R2R fabrication is presented in fig. S24. Scale bars: 2 cm. Photo credit: Seo Woo Song and Sumin Lee, Seoul National University.

these aspects, we determined the optimal condition for SCIRP to be 40 wt % of 5-μm iron microparticles in the floating ink with 3-min incubation.

The final 3D structures were controlled by not only the design of the initial 2D drawing but also the depth of the monomer solution (Fig. 3D). Here, polymers including rhodamine B were used, and images were captured under blue-ultraviolet (UV) light to better visualize the transformations (fig. S20). Figure 3E shows various 3D structures and their initial 2D precursor designs. When demonstrating the pop-up letters "SNU," we implemented a sacrificial layer that disappeared after the SCIRP process by excluding iron microparticles from the floating ink (Fig. 3E, bottom right, and fig. S21).

Pen-based 4D printing

A pen-based approach allows for a high degree of freedom when selecting a printing substrate. We further demonstrated that pen-based 4D printing can be applied to fabricate 3D structures on various substrates, including glass, plastic, poly(dimethylsiloxane) (PDMS), ceramic, metal, curved surfaces, and even on natural substrates such as stone and leaf (Fig. 4A, fig. S22, and movie S7). This enables 3D fabrication in locations that are difficult to print on using conventional 3D printing systems. Furthermore, on-site reconfiguration is made possible by drawing a 2D precursor on a thin and flexible substrate, which allows for the fabrication of 3D structures inside narrow spaces that are difficult to directly fabricate with

conventional 3D printers. We drew a precursor on a thin PDMS film and transformed it into a pop-up structure inside a bottle whose neck was narrower than the pop-up structure, also known as an "impossible bottle" (Fig. 4B). We achieved this through a simple process of drawing, rolling, loading, placing, and floating the precursor. Because the initial precursors have a much smaller volume than the final products, pen-based 4D printing enables easy and dense packaging and delivery. Because pen-based 4D printing can be used with a variety of substrates, on-site manufacturing is also possible and provides for a wide range of possibilities, including rapid modification of 3D designs, overprinting (53), and even "3D printing anywhere."

Last, we used roll-to-roll (R2R) processing with pen-based 4D printing to demonstrate the rapid mass production of 3D objects on a large area of thin and flexible polyvinyl chloride film (Fig. 4C and figs. S23 and S24). Conventional 3D manufacturing technologies have a trade-off between high throughput (e.g., injection molding) (54–56) and rapid prototyping availability (e.g., 3D printer) (53, 57–59). The simplicity of pen-based 4D printing allows for integration with R2R methods, thereby overcoming the current trade-off. To achieve continuous R2R processing, we installed a pen plotter for 2D printing of the initial precursors and a monomer solution bath for 3D formation. As the film progressed through the system, the pen-drawn precursors entered the monomer solution and transformed into 3D structures. The transformed 3D shapes were fixed via SCIRP in the monomer solution bath before emerging from the

bath. Using this R2R setup, we could make 60 copies of 3D objects in a human-scale large area within 30 min. The shape of 3D objects fabricated by R2R fabrication (fig. S24A) was not as consistent as those produced by one-by-one fabrication (fig. S24B). However, we believe that the uniformity of the R2R system can be further improved if automation for this process is accomplished. Despite the fact that the current system presented here is not fully automated, we believe that the R2R 3D fabrication has a substantial potential to provide new possibilities in a rapid and mass 3D fabrication.

DISCUSSION
Pen-based 4D printing is an easy and intuitive 3D fabrication method based on 2D pen drawing. The most attractive feature of 4D printing is its potential to construct 3D structures from lower-dimensional printed structures that can lower the manufacturing time and cost. However, 3D printing or multistep fabrication has been generally considered essential for conventional 4D printing technology as their shape morphing mechanisms need multilayer structures to induce asymmetric stress generated by local volume change of responsive materials (60). We have developed STAT as a novel shape morphing mechanism, which is based on real 2D-to-3D transformation, widening the variety of 4D printing mechanisms. Our pen-based 4D printing requires only a marker pen that is much simpler and faster than a 3D printer. Although pen-based 4D printing is limited to geometry with two anchoring surfaces, it allows freestyle 3D fabrication not limited to the certain substrate by adopting the pen as a 3D fabrication interface. These advantages lead to the presented technology's potential for the accessible and rapid fabrication to be applied in various fields including electrical applications (fig. S25), soft robotics (fig. S26), and bio-applications (fig. S27). We anticipate that this study may enable further development of simple and efficient techniques for 3D fabrication via 2D-based technologies and further expand the value of 4D printing.

MATERIALS AND METHODS
Preparation of floating ink, anchoring ink, and pens
The floating ink we used in this work was developed based on the commercial dry-erase marker (50). To the best of our knowledge, every commercialized dry-erase marker drawing generates PVB film after the ink dries, and the PVB film floats on the surface of water when the PVB film encounters water due to the hydrophilic-hydrophobic interaction. However, public data showing the exact composition of the commercial dry-erase marker do not exist (maybe due to the confidential information); thus, we blended our custom floating ink based on the patent from a Korean company, "Inc. Highline" (50). After optimizing the composition of the floating ink considering the physical properties of the ink and the PVB film (figs. S4 and S5), the exact composition of the floating ink and anchoring ink was chosen as shown in fig. S3.

PVB, dibutyl sebacate, triethylene glycol monobutyl ether, 2-(diethylamino) ethanol, butyl stearate, and Tween 20 were purchased from Sigma-Aldrich. The color of the ink can be freely determined according to the color of the pigment (fig. S2 and movie S2). For consistency, red and black pigments were used for the floating ink and anchoring ink, respectively, unless otherwise noted. In Fig. 4A and fig. S22, the floating ink with green pigment was used to express frog and human eyes. Red, black, and green pigments used in this study were C.I. pigment red 254, Solvent black 5, and C.I. pigment green 7, respectively, purchased from Tokyo Chemical Industry. Ethanol (EtOH) and isopropyl alcohol mixed in 8:2 ratio were prepared as solvent.

All materials were poured in a 50-ml conical tube depending on the predetermined composition, and then the solution was vortexed at a speed of 1000 rpm over 24 hours. Prepared ink was poured into the empty pen to prepare drawing. Various widths of empty pens were used. <Montana Acrylic Empty, 0.7 mm Paint Marker> was used in fig. S8A, <Baosity Oil Acrylic Paints Marker Pen Empty Tube Ink Fountain Refill Pen—0.7-mm Tips> was used in fig. S8B, <Molotow ONE4ALL Empty Acrylic Paint Marker (2 mm)> was used in fig. S8C, and <Green Board empty pen (3-mm nib, from Green B&T, Korea)> was used in fig. S8D. Unless stated otherwise, all data in the manuscript were generated using the Green Board empty pen with 3-mm nib.

Structural reinforcement by SCIRP
For the structural reinforcement, the 3D structure made of PVB film is coated with a hydrogel layer by iron microparticle–mediated SCIRP. The floating ink was mixed with 40 wt % of iron microparticles. The monomer solution for SCIRP was prepared by mixing KPS (2 mg/ml; Sigma-Aldrich) and 25% (v/v) of poly(ethylene glycol) diacrylate (PEGDA; average Mn 700, Sigma-Aldrich) in water. Here, 5 μm of iron microparticles (U.S. Research Nanomaterials Inc.) was used unless otherwise stated, and 40 nm of iron nanoparticles was used for the experiments shown in fig. S19.

As described in Fig. 3A, iron microparticles embedded in PVB film accelerate the decomposition of persulfate ions in solution, thereby generating free radicals nearby the PVB film. These free radicals induce cross-linking of monomer in the solution near iron microparticles (Fig. 1C and movie S5). In Figs. 3 and 4 (B and C), Rhodamine B (Sigma-Aldrich) was used for better visualization (fig. S15).

In case of the portions of the PVB film floating on the monomer solution, polymer coating on the bottom portions was initiated before the polymer coating on the upper portion because the upper portions exposed to the air did not contact the monomer solution. To coat both the upper bottom portions of the floating film, we added some monomer solution 1 min later, so that the whole structures were submerged to the monomer solution.

Measuring thickness and mechanical properties of materials
To optimize the mechanical properties of the PVB film and to take simulation parameters, we obtained the load-displacement curve of PVB films. Previously, we developed a nano-UTM that can perform tensile tests on water surface (fig. S4B) (51). This device was developed to measure very thin and delicate samples, which are difficult to be transferred or loaded on a template of nano-UTM machine. Using this nano-UTM device, the thin film can be easily loaded on device without deformation of samples because of the water-assisted transfer. In addition, the mechanical properties of the PVB film may vary depending on the surrounding environment. Because this device performs a tensile test on the water surface, the mechanical properties of the PVB film can be measured in an environment most similar to the actual environment in which the 3D structures of the PVB film is transformed in water.

To measure the PVB film through the nano-UTM device, first we printed a dog-bone shape on a glass slide with a pen filled with the floating ink and then floated the sample on the water surface.

The dimension of the dog-bone shape is shown in fig. S4A. Both grips of sample were attached to the PDMS-coated grips of nano-UTM by van der Waals forces. We extended the sample until fracture occurred while measuring the load (fig. S4C). The displacement and loading force were measured from linear motor (LPS-24, PI) and load cell (LTS-50GA, KYOWA), respectively, embedded on the nano-UTM device. The fracture strain was calculated from charge-coupled device images of the PVB film gauge during the measurement process.

To compare the mechanical properties of PVB films before and after the SCIRP process, we also measured the sample coated with the hydrogel layer by the SCIRP process. Because the hydrogel layer on the samples is very slippery and makes it difficult to be attached on the PDMS-coated grip, we used UV-curable adhesive [Norland Optical Adhesive 61 (NOA 61)] to immobilize the sample on the nano-UTM device (fig. S4B).

The thickness of the PVB film (before SCIRP), which was about 1 μm, was measured by atomic force microscopy (NX-10, Park Systems). The thickness of the hydrogel-coated PVB film (after SCIRP) was measured by the method described in fig. S16. Briefly, first, we drew a line with Fe-including ink, and the polymer layer was coated on the film by the SCIRP process (fig. S16, A and B). To obtain the microscopy image of the cross section of the hydrogel-coated PVB film, we used a PDMS block, inspired by the paraffin block in a biology study (fig. S16, C and D, and Fig. 3B).

Computational design and printing

Pen-based 4D printing can take advantage of both drawing and printing. For the precise design and mass production with high reproducibility, we used CAD software, Inkscape, and a commercialized automatic pen plotter (Axidraw V3, Evil Mad Scientist) (Fig. 2C, fig. S6, and movie S1). Using Axidraw plug-in software in Inkscape, the design we drew on the computer could be easily printed out by a pen plotter.

Simulation of structural transformation

Finite element simulations were performed using commercially available FEA software ABAQUS to predict the morphology change of the printed structures. To simplify the model for observation of the macroscopic deformation, the surface tension was bypassed and replaced with the reactive normal force of a rigid membrane placed above structures while structures were under an upward gravitational load. Then, the rigid membrane was gradually elevated to characterize the increment of the water level.

In all structures, 3D deformable continuum shell models were built with finite-strain shell elements of type S4R with a uniform thickness of 1 μm. The structures were partitioned into anchoring and floating sections corresponding to the original design, and all displacements and rotations were constrained for the anchoring sections. The material of the structures was modeled as a linear elastic model for simplified simulation with the following experimentally measured input parameters: the density $d = 1.33$ g/cm^3, the Young's modulus $E = 650$ kPa, and the Poisson's ratio $\nu = 0.495$, unless otherwise stated. However, in the case of the structure shown in the top panel of Fig. 2D, the maximum strain exceeded 17%, which is the transition value of the linear elastic and nonlinear region of the film. For this structure, we performed the simulation using real strain-stress data shown in fig. S4. The gravitational acceleration value was determined by fitting the simulation results to the actual deformation results through transformation of a simple structure (fig. S9). With optimal value of gravitational acceleration ($G = 2000$), simulation results were almost similar to the actual transformation.

R2R fabrication of pen-based 4D printing

The R2R manufacturing setup of pen-based 4D printing was demonstrated to represent the potential of the pen-based 4D printing for mass production of 3D objects (Fig. 4C and fig. S23). R2R availability represents the industrial applicability of pen-based 4D printing and simplicity of the manufacturing process. The R2R setup was composed of a 2D printer (pen plotter), a computer for controlling the 2D printer, and a monomer solution tray (fig. S23). Because of the dimension limitation of the pen plotter, the width of the substrate roll was determined to be 30 cm. After the printing step, 2D drawings on the film are dipped into the tray filled with monomer solution for 5 min for structure fixation. When the 2D drawings encounter the solution, they are spontaneously transformed into their designated 3D structure. During the incubation time for structure fixation, the pen plotter carries out the printing on the following area. Because our pen plotter only supports single-pen mode, we printed the floating part first and then replaced the pen to draw the anchoring part. After 5 min, the film moves 25 cm in the direction of progress, and the same processes are repeated under each part. Using this R2R setup, we could print 60 copies of 3D objects on a human-scale large-area substrate (30 cm by 150 cm) within 30 min (Fig. 4C). In the experiment described in fig. S24, 36 copies of 3D objects were fabricated within 20 min.

SUPPLEMENTARY MATERIALS

Supplementary material for this article is available at http://advances.sciencemag.org/cgi/content/full/7/13/eabf3804/DC1

REFERENCES AND NOTES

1. Y. Liu, J. Genzer, M. D. Dickey, "2D or not 2D": Shape-programming polymer sheets. *Prog. Polym. Sci.* **52**, 79–106 (2016).
2. Y. Sun, W. M. Choi, H. Jiang, Y. Y. Huang, J. A. Rogers, Controlled buckling of semiconductor nanoribbons for stretchable electronics. *Nat. Nanotechnol.* **1**, 201–207 (2006).
3. S. Felton, M. Tolley, E. Demaine, D. Rus, R. Wood, A method for building self-folding machines. *Science* **345**, 644–646 (2014).
4. B. J. Cafferty, V. E. Campbell, P. Rothemund, D. J. Preston, A. Ainla, N. Fulleringer, A. C. Diaz, A. E. Fuentes, D. Sameoto, J. A. Lewis, G. M. Whitesides, Fabricating 3D structures by combining 2D printing and relaxation of strain. *Adv. Mater. Technol.* **4**, 1800299 (2019).
5. Y. Liu, B. Shaw, M. D. Dickey, J. Genzer, Sequential self-folding of polymer sheets. *Sci. Adv.* **3**, e1602417 (2017).
6. Y. Liu, J. K. Boyles, J. Genzer, M. D. Dickey, Self-folding of polymer sheets using local light absorption. *Soft Matter* **8**, 1764–1769 (2012).
7. S. Sundaram, D. S. Kim, M. A. Baldo, R. C. Hayward, W. Matusik, 3D-printed self-folding electronics. *ACS Appl. Mater. Interfaces* **9**, 32290–32298 (2017).
8. C. Py, P. Reverdy, L. Doppler, J. Bico, B. Roman, C. N. Baroud, Capillary origami: Spontaneous wrapping of a droplet with an elastic sheet. *Phys. Rev. Lett.* **98**, 156103 (2007).
9. Z. Zhao, J. Wu, X. Mu, H. Chen, H. J. Qi, D. Fang, Origami by frontal photopolymerization. *Sci. Adv.* **3**, e1602326 (2017).
10. J.-H. Na, A. A. Evans, J. Bae, M. C. Chiappelli, C. D. Santangelo, R. J. Lang, T. C. Hull, R. C. Hayward, Programming reversibly self-folding origami with micropatterned photo-crosslinkable polymer trilayers. *Adv. Mater.* **27**, 79–85 (2015).
11. K. Kuribayashi-Shigetomi, H. Onoe, S. Takeuchi, Cell origami: Self-folding of three-dimensional cell-laden microstructures driven by cell traction force. *PLOS ONE* **7**, e51085 (2012).
12. Z. Liu, H. Du, J. Li, L. Lu, Z.-Y. Li, N. X. Fang, Nano-kirigami with giant optical chirality. *Sci. Adv.* **4**, eaat4436 (2018).
13. K. Nan, H. Luan, Z. Yan, X. Ning, Y. Wang, A. Wang, J. Wang, M. Han, M. Chang, K. Li, Y. Zhang, W. Huang, Y. Xue, Y. Huang, Y. Zhang, J. A. Rogers, Engineered elastomer substrates for guided assembly of complex 3D mesostructures by spatially nonuniform compressive buckling. *Adv. Funct. Mater.* **27**, 1604281 (2017).
14. Z. Yan, F. Zhang, F. Liu, M. Han, D. Ou, Y. Liu, Q. Lin, X. Guo, H. Fu, Z. Xie, M. Gao, Y. Huang, J. H. Kim, Y. Qiu, K. Nan, J. Kim, P. Gutruf, H. Luo, A. Zhao, K.-C. Hwang, Y. Huang, Y. Zhang,

J. A. Rogers, Mechanical assembly of complex, 3D mesostructures from releasable multilayers of advanced materials. *Sci. Adv.* **2**, e1601014 (2016).

15. H. Fu, K. Nan, W. Bai, W. Huang, K. Bai, L. Lu, C. Zhou, Y. Liu, F. Liu, J. Wang, M. Han, Z. Yan, H. Luan, Y. Zhang, Y. Zhang, J. Zhao, X. Cheng, M. Li, J. W. Lee, Y. Liu, D. Fang, X. Li, Y. Huang, Y. Zhang, J. A. Rogers, Morphable 3D mesostructures and microelectronic devices by multistable buckling mechanics. *Nat. Mater.* **17**, 268–276 (2018).

16. S. Xu, Z. Yan, K.-I. Jang, W. Huang, H. Fu, J. Kim, Z. Wei, M. Flavin, J. M. Cracken, R. Wang, A. Badea, Y. Liu, D. Xiao, G. Zhou, J. Lee, H. U. Chung, H. Cheng, W. Ren, A. Banks, X. Li, U. Paik, R. G. Nuzzo, Y. Huang, Y. Zhang, J. A. Rogers, Assembly of micro/nanomaterials into complex, three-dimensional architectures by compressive buckling. *Science* **347**, 154–159 (2015).

17. W. Miao, W. Zou, B. Jin, C. Ni, N. Zheng, Q. Zhao, T. Xie, On demand shape memory polymer via light regulated topological defects in a dynamic covalent network. *Nat. Commun.* **11**, 4257 (2020).

18. L. Cera, G. M. Gonzalez, Q. Liu, S. Choi, C. O. Chantre, J. Lee, R. Gabardi, M. C. Choi, K. Shin, K. K. Parker, A bioinspired and hierarchically structured shape-memory material. *Nat. Mater.* **20**, 242–249 (2021).

19. Z. Ding, C. Yuan, X. Peng, T. Wang, H. J. Qi, M. L. Dunn, Direct 4D printing via active composite materials. *Sci. Adv.* **3**, e16022890 (2017).

20. B. Jin, H. Song, R. Jiang, J. Song, Q. Zhao, T. Xie, Programming a crystalline shape memory polymer network with thermo- and photo-reversible bonds toward a single-component soft robot. *Sci. Adv.* **4**, eaao3865 (2018).

21. D. Raviv, W. Zhao, C. M. Knelly, A. Papadopoulou, A. Kadambi, B. Shi, S. Hirsch, D. Dikovsky, M. Zyracki, C. Olguin, R. Raskar, S. Tibbits, Active printed materials for complex self-evolving deformations. *Sci. Rep.* **4**, 7422 (2014).

22. L. Huang, R. Jiang, J. Wu, J. Song, H. Bai, B. Li, Q. Zhao, T. Xie, Ultrafast digital printing toward 4D shape changing materials. *Adv. Mater.* **29**, 1605390 (2017).

23. J. W. Boley, W. M. van Rees, C. Lissandrello, M. N. Horenstein, R. L. Truby, A. Kotikian, J. A. Lewis, L. Mahadevan, Shape-shifting structured lattices via multimaterial 4D printing. *Proc. Natl. Acad. Sci. U.S.A.* **116**, 20856–20862 (2019).

24. A. Sydney Gladman, E. A. Matsumoto, R. G. Nuzzo, L. Mahadevan, J. A. Lewis, Biomimetic 4D printing. *Nat. Mater.* **15**, 413–418 (2016).

25. Y. Kim, H. Yuk, R. Zhao, S. A. Chester, X. Zhao, Printing ferromagnetic domains for untethered fast-transforming soft materials. *Nature* **558**, 274–279 (2018).

26. Y. Alapan, A. C. Karacakol, S. N. Guzelhan, I. Isik, M. Sitti, Reprogrammable shape morphing of magnetic soft machines. *Sci. Adv.* **6**, eabc6414 (2020).

27. J. J. Schwartz, A. J. Boydston, Multimaterial actinic spatial control 3D and 4D printing. *Nat. Commun.* **10**, 791 (2019).

28. G. Liu, Y. Zhao, G. Wu, J. Lu, Origami and 4D printing of elastomer-derived ceramic structures. *Sci. Adv.* **4**, eaat0641 (2018).

29. Z. Li, H. Liu, C. Ouyang, W. Hong Wee, X. Cui, T. Jian Lu, B. Pingguan-Murphy, F. Li, F. Xu, Recent advances in pen-based writing electronics and their emerging applications. *Adv. Funct. Mater.* **26**, 165–180 (2016).

30. A. W. Martinez, S. T. Phillips, B. J. Wiley, M. Gupta, G. M. Whitesides, FLASH: A rapid method for prototyping paper-based microfluidic devices. *Lab Chip* **8**, 2146–2150 (2008).

31. R. Amin, F. Ghaderinezhad, L. Li, E. Lepowsky, B. Yenilmez, S. Knowlton, S. Tasoglu, Continuous-ink, multiplexed pen-plotter approach for, high-throughput fabrication of paper-based microfluidics. *Anal. Chem.* **89**, 6351–6357 (2017).

32. O. Rahmanian, D. L. Devoe, Pen microfluidics: Rapid desktop manufacturing of sealed thermoplastic microchannels. *Lab Chip* **13**, 1102–1108 (2013).

33. E. J. Walsh, A. Feuerborn, J. H. R. Wheeler, A. N. Tan, W. M. Durham, K. R. Foster, P. R. Cook, Microfluidics with fluid walls. *Nat. Commun.* **8**, 819 (2017).

34. A. Russo, B. Y. Ahn, J. J. Adams, E. B. Duoss, J. T. Bernhard, J. A. Lewis, Pen-on-paper flexible electronics. *Adv. Mater.* **23**, 3426–3430 (2011).

35. S. Liu, J. Li, X. Shi, E. Gao, Z. Xu, H. Tang, K. Tong, Q. Pei, J. Liang, Y. Chen, Rollerball-pen-drawing technology for extremely foldable paper-based electronics. *Adv. Electron. Mater.* **3**, 1700098 (2017).

36. M. Hu, X. Cai, Q. Guo, B. Bian, T. Zhang, J. Yang, Direct pen writing of adhesive particle-free ultrahigh silver salt-loaded composite ink for stretchable circuits. *ACS Nano* **10**, 396–404 (2016).

37. X. Liao, Q. Liao, X. Yan, Q. Liang, H. Si, M. Li, H. Wu, S. Cao, Y. Zhang, Flexible and highly sensitive strain sensors fabricated by pencil drawn for wearable monitor. *Adv. Funct. Mater.* **25**, 2395–2401 (2015).

38. A. J. Bandodkar, W. Jia, J. Ramírez, J. Wang, Biocompatible enzymatic roller pens for direct writing of biocatalytic materials: "Do-it-Yourself" electrochemical biosensors. *Adv. Healthc. Mater.* **4**, 1215–1224 (2015).

39. S.-M. Jeong, T. Lim, J. Park, C.-Y. Han, H. Yang, S. Ju, Pen drawing display. *Nat. Commun.* **10**, 4334 (2019).

40. M. Zhang, B. Hu, L. Meng, R. Bian, S. Wang, Y. Wang, H. Liu, L. Jiang, Ultrasmooth quantum dot micropatterns by a facile controllable liquid-transfer approach: Low-cost fabrication of high-performance QLED. *J. Am. Chem. Soc.* **140**, 8690–8695 (2018).

41. T. Walker, P. Dilworth, M. Bogue, D. Cowen, Drawing tool, U.S. Patent 749173S1 (2014).

42. S. Khodaparast, F. Boulogne, C. Poulard, H. A. Stone, Water-based peeling of thin hydrophobic films. *Phys. Rev. Lett.* **119**, 154502 (2017).

43. J. W. Obreimoff, The splitting strength of mica. *Proc. R. Soc. London. Ser. A* **127**, 290–297 (1930).

44. K. Kendall, Thin-film peeling-the elastic term. *J. Phys. D Appl. Phys.* **8**, 1449–1452 (1975).

45. Y. Zhang, M. Yin, Y. Baek, K. Lee, G. Zangari, L. Cai, B. Xu, Capillary transfer of soft films. *Proc. Natl. Acad. Sci. U.S.A.* **117**, 5210–5216 (2020).

46. J. Yan, A. Moreau, S. Khodaparast, A. Perazzo, J. Feng, C. Fei, S. Mao, S. Mukherjee, A. Košmrlj, N. S. Wingreen, B. L. Bassler, H. A. Stone, Bacterial biofilm material properties enable removal and transfer by capillary peeling. *Adv. Mater.* **30**, 1804153 (2018).

47. X. Ma, Q. Liu, D. Xu, Y. Zhu, S. Kim, Y. Cui, L. Zhong, M. Liu, Capillary-force-assisted clean-stamp transfer of two-dimensional materials. *Nano Lett.* **17**, 6961–6967 (2017).

48. H. Zhang, Y. Liu, C. Yang, L. Xiang, Y. Hu, L. Peng, Wafer-scale fabrication of ultrathin flexible electronic systems via capillary-assisted electrochemical delamination. *Adv. Mater.* **30**, 1805408 (2018).

49. S. Ma, C. Yan, M. Cai, J. Yang, X. Wang, F. Zhou, W. Liu, Continuous surface polymerization via Fe(II)-mediated redox reaction for thick hydrogel coatings on versatile substrates. *Adv. Mater.* **30**, 1803371 (2018).

50. G.-S. Jeon, S.-E. Park, "Ink composition for board marker," South Korea Patent 101227060B1 (2013).

51. S. Chen, S. Jung, H. J. Cho, N. H. Kim, S. Jung, J. Xu, J. Oh, Y. Cho, H. Kim, B. Lee, Y. An, C. Zhang, M. Xiao, H. Ki, Z. G. Zhang, J. Y. Kim, Y. Li, H. Park, C. Yang, Highly flexible and efficient all-polymer solar cells with high-viscosity processing polymer additive toward potential of stretchable devices. *Angew. Chem. Int. Ed.* **57**, 13277–13282 (2018).

52. J.-H. Kim, J. Noh, H. Choi, J.-Y. Lee, T.-S. Kim, Mechanical properties of polymer-fullerene bulk heterojunction films: Role of nanomorphology of composite films. *Chem. Mater.* **29**, 3954–3961 (2017).

53. B. E. Kelly, I. Bhattacharya, H. Heidari, M. Shusteff, C. M. Spadaccini, H. K. Taylor, Volumetric additive manufacturing via tomographic reconstruction. *Science* **363**, 1075–1079 (2019).

54. J. Giboz, T. Copponnex, P. Mélé, Microinjection molding of thermoplastic polymers: A review. *J. Micromech. Microeng.* **17**, R96–R109 (2007).

55. E. Berthier, E. W. K. Young, D. Beebe, Engineers are from PDMS-land, biologists are from Polystyrenia. *Lab Chip* **12**, 1224–1237 (2012).

56. E. Sollier, C. Murray, P. Maoddi, D. Di Carlo, Rapid prototyping polymers for microfluidic devices and high pressure injections. *Lab Chip* **11**, 3752–3765 (2011).

57. J. R. Tumbleston, D. Shirvanyants, N. Ermoshkin, R. Janusziewicz, A. R. Johnson, D. Kelly, K. Chen, R. Pinschmidt, J. P. Rolland, A. Ermoshkin, E. T. Samulski, J. M. DeSimone, Continuous liquid interface production of 3D objects. *Science* **347**, 1349–1352 (2015).

58. D. A. Walker, J. L. Hedrick, C. A. Mirkin, Rapid, large-volume, thermally controlled 3D printing using a mobile liquid interface. *Science* **366**, 360–364 (2019).

59. M. A. Skylar-Scott, J. Mueller, C. W. Visser, J. A. Lewis, Voxelated soft matter via multimaterial multinozzle 3D printing. *Nature* **575**, 330–335 (2019).

60. X. Kuang, D. J. Roach, J. Wu, C. M. Hamel, Z. Ding, T. Wang, M. L. Dunn, H. J. Qi, Advances in 4D printing: Materials and applications. *Adv. Funct. Mater.* **29**, 1805290 (2019).

Citation: S. W. Song, S. Lee, J. K. Choe, N.-H. Kim, J. Kang, A. C. Lee, Y. Choi, A. Choi, Y. Jeong, W. Lee, J.-Y. Kim, S. Kwon, J. Kim, Direct 2D-to-3D transformation of pen drawings. *Sci. Adv.* **7**, eabf3804 (2021).

Science Advances

Direct 2D-to-3D transformation of pen drawings

Seo Woo Song, Sumin Lee, Jun Kyu Choe, Na-Hyang Kim, Junwon Kang, Amos Chungwon Lee, Yeongjae Choi, Ahyoun Choi, Yunjin Jeong, Wooseok Lee, Ju-Young Kim, Sunghoon Kwon and Jiyun Kim

ARTICLE TOOLS	http://advances.sciencemag.org/content/7/13/eabf3804
SUPPLEMENTARY MATERIALS	http://advances.sciencemag.org/content/suppl/2021/03/22/7.13.eabf3804.DC1
REFERENCES	This article cites 58 articles, 14 of which you can access for free http://advances.sciencemag.org/content/7/13/eabf3804#BIBL
PERMISSIONS	http://www.sciencemag.org/help/reprints-and-permissions

Use of this article is subject to the Terms of Service